remote sensing

MDPI

Article

Estimation of Glacier Mass Balance in the Three-River Headwaters Region from 2000 to 2025 Based on ZiYuan-3 Satellite Data

Da Liang, Lin Liu *, Yu Liao, Xueyu Zhang, Zhengwei Li, Haihang Jing and Zhicai Luo

National Gravitation Laboratory, MOE Key Laboratory of Fundamental Physical Quantities Measurement, School of Physics, Huazhong University of Science and Technology, Wuhan 430074, China; liangda@hust.edu.cn (D.L.)
* Correspondence: liulin616@hust.edu.cn

Highlights

What are the main findings?

- From 2000 to 2025, glaciers in the Three-River Headwaters Region exhibited an overall negative mass balance with strong spatial heterogeneity; the most severe mass loss occurred in the Lancang River source (-0.70 ± 0.07 m w.e. yr^{-1}), while the Yellow River source showed the mildest loss (-0.37 ± 0.09 m w.e. yr^{-1}).
- Compared with pre-2018 estimates, glacier mass loss accelerated notably after 2018, with rising air temperature playing a dominant role compared to increased precipitation in driving the accelerated ablation.

What are the implications of the main findings?

- The direct contribution of glacier mass loss to annual river runoff in the Three-River Headwaters Region is less than 2%, indicating that regional runoff is primarily controlled by precipitation rather than glacier meltwater.
- The high-precision geodetic method based on ZiYuan-3 stereo imagery and SRTM DEM effectively captures spatially heterogeneous glacier changes, providing a scientific basis for water resource management and ecological conservation in this critical "Asian Water Tower" region.

Abstract

Under the background of global climate warming, glaciers in the Three-River Headwaters Region, as a crucial component of the "Asian Water Tower," exert profound influences on regional water resource security and ecological stability through their mass balance variations. Due to the scarcity of in situ observations caused by the harsh high-altitude environment, long-term monitoring based on remote sensing techniques is urgently required. In this study, the geodetic method was employed, using the SRTM-C DEM acquired in 2000 as the reference, and recent glacier surface DEMs were generated from high-resolution ZiYuan-3 tri-stereo imagery obtained during 2024–2025. Through refined DEM co-registration, differencing, and systematic error corrections, the glacier mass balance in the Three-River Headwaters Region from 2000 to 2025 was systematically estimated. The results indicate that the glaciers in the study area exhibited an overall negative mass balance during the study period, with significant spatial heterogeneity. Among the sub-regions, the Lancang River source region experienced the most pronounced mass loss (-0.70 ± 0.07 m w.e. yr^{-1}), whereas the Yellow River source region showed the lowest mass loss (-0.37 ± 0.09 m w.e. yr^{-1}). Compared with earlier studies, glacier mass loss has accelerated in recent years and is closely associated with regional climatic characteristics. This study provides a scientific

Academic Editor: Yi Luo

Received: 21 May 2026
Revised: 15 June 2026
Accepted: 30 June 2026
Published: 2 July 2026

basis for understanding glacier changes and their hydrological and ecological impacts in the Three-River Headwaters Region.

Keywords: Three-River Headwaters Region; glacier mass balance; geodetic method; SRTM; ZiYuan-3; climate change

1. Introduction

The Three-River Headwaters Region is located in the hinterland of the Qinghai–Tibet Plateau and serves as the source region of the Yangtze River, Yellow River, and Lancang River. It is widely known as the "Asian Water Tower." This region is not only an important ecological security barrier of China but also a key area for maintaining water resource security and sustainable socio-economic development in downstream regions. In 2003, the Three-River Headwaters Nature Reserve was officially established and was upgraded to a national park in 2020, highlighting its prominent role in the national ecological conservation strategy. Under the background of global climate warming, glaciers in this region, acting as sensitive climate indicators and regulators of water resources, directly affect regional hydrological processes and ecological stability. Therefore, long-term monitoring and mechanism studies of glacier mass balance in this region are of great scientific significance and national strategic value [1–3].

In recent years, with the rapid development of remote sensing technology, glacier mass balance studies based on the geodetic method have become an important approach for assessing glacier changes [4,5]. At present, numerous studies have been conducted on glaciers in the Qinghai–Tibet Plateau and its surrounding regions, achieving significant progress in both methodology and application [6]. For example, Liu et al. used ZiYuan-3 (ZY-3) stereo imagery and SRTM DEM data to estimate glacier mass balance in the source region of the Yangtze River from 2000 to 2018, revealing an overall negative mass balance with significant spatial heterogeneity [7]. Similar geodetic approaches based on DEM differencing have been successfully applied to other glacierized regions on the Tibetan Plateau, such as the Yulong Snow Mountain [8]. In addition to geodetic methods, energy balance models have been successfully applied to quantify glacier mass balance and its climate sensitivity at the glacier scale [9]. However, similar studies are mostly limited to periods before 2018 and are often confined to individual basins or local regions. Systematic investigations covering the entire Three-River Headwaters Region, especially for the recent period from 2000 to 2025, remain relatively scarce [10].

To address these research gaps, this study conducts a systematic assessment of glacier mass balance across the entire Three-River Headwaters Region for the period 2000–2025. The geodetic method is employed, using the SRTM-C DEM from early 2000 as the reference, and recent glacier surface DEMs are generated from multi-scene high-resolution ZY-3 tri-stereo optical imagery acquired during 2024–2025. Through refined DEM co-registration, differencing, and systematic error corrections, glacier surface elevation changes during the study period are derived, and the mass balance of glaciers in each subregion is subsequently estimated. By incorporating radar penetration correction, resolution difference correction, and seasonal bias correction, this study improves the accuracy and reliability of mass balance estimation [11]. In addition, by integrating meteorological data, the driving mechanisms of glacier changes are explored to reveal the spatiotemporal evolution characteristics of glacier mass balance in the Three-River Headwaters Region and its response to climate change, thereby providing a scientific basis for regional water resource management and ecological conservation.

2. Study Area

The Three-River Headwaters Region (TRHR) is located in the central-eastern Qinghai–Tibet Plateau (89°45′–102°23′ E, 31°39′–36°12′ N) and administratively belongs to southern Qinghai Province. As the source region of the Yangtze River, Yellow River, and Lancang River, it constitutes the core component of the Asian Water Tower and serves as a critical ecological security barrier and water conservation area for China and Asia. It also plays a key role in the atmospheric circulation system of the Northern Hemisphere [12–14]. The terrain of the region is dominated by plateaus and mountain ranges, with an average elevation of approximately 4500 m, gradually increasing from southeast to northwest and reaching a maximum elevation of 6824 m. The major mountain ranges include the Kunlun Mountains in the north, the Bayan Har Mountains in the central region, the Animaqing Mountains in the east, and the Tanggula Mountains in the south, forming the fundamental topographic framework of the region (Figure 1). Influenced by its high altitude and complex terrain, the region exhibits a typical plateau continental climate, which can be broadly divided into two distinct seasons throughout the year. The cold season (approximately October to April of the following year) is dominated by the Qinghai–Tibet Plateau high-pressure system, characterized by cold and dry conditions with scarce precipitation. In contrast, the ablation season (May to September) experiences rising temperatures and relatively concentrated precipitation, representing the primary period of glacier accumulation and ablation.

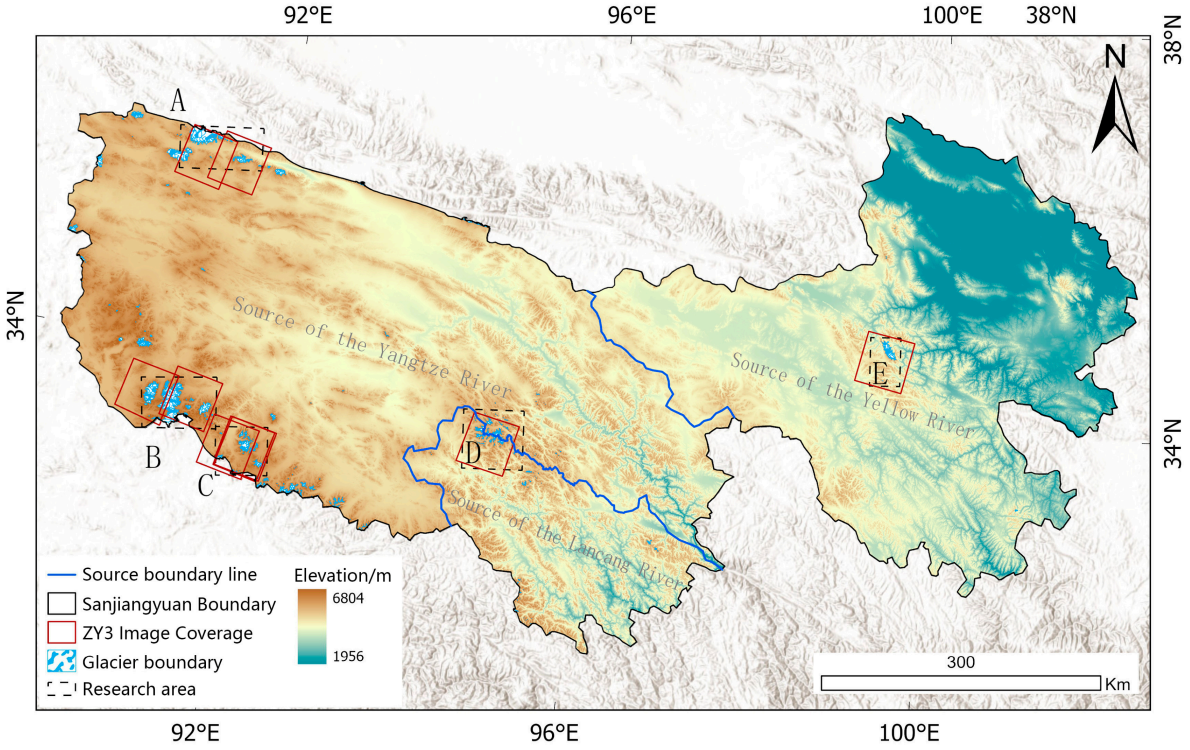

Figure 1. Geographic location, glacier distribution, and the five selected study regions in the TRHR. (The blue area indicates glacier distribution based on the Randolph Glacier Inventory (RGI 7.0); A–E represent the five study regions: Kunlun, Geladandong, Dongkemadi, Serfeng, and Animaqing, respectively).

The core focus of this study is the glacier system within this region. According to the Second Chinese Glacier Inventory, glaciers are widely distributed across the aforementioned mountain ranges, with concentrated distributions on the northern slope of the Tanggula Mountains, the southern slope of the Kunlun Mountains, and in areas such as Serfeng [15]. To systematically and representatively assess glacier mass balance across the entire Three-

River Headwaters Region, five key study regions were selected based on considerations of spatial coverage and topographic–climatic representativeness (Figure 1): the Kunlun region (southern slope of the Kunlun Mountains at the northern margin of the Yangtze River source), the Geladandong region (main peak area of the Tanggula Mountains in the Yangtze River source), the Dongkemadi region (central Tanggula Mountains in the Yangtze River source), the Serfeng region (a major glacierized area in the Lancang River source), and the Animaqing Mountains (glaciers in the Yellow River source). These five regions encompass diverse climatic and topographic units from south to north and from east to west, and their glacier variations effectively reflect the overall spatial heterogeneity of glaciers in the Three-River Headwaters Region. Glaciers in all regions are characterized as the summer-accumulation type, with the accumulation and ablation processes primarily occurring during the ablation season. Their mass variations directly respond to changes in ablation season temperature and solid precipitation.

3. Data and Methods

3.1. Data Sets

This study aims to obtain glacier surface elevation changes in the Three-River Headwaters Region from 2000 to 2025 using the geodetic method. The core of this method is to compare digital elevation models (DEMs) from two different periods. Therefore, two sets of spaceborne DEM data were employed: the SRTM DEM acquired in early 2000 as the reference topographic dataset, and a recent glacier surface DEM generated from high-resolution ZY-3 tri-stereo optical imagery acquired during 2024–2025.

The ZY-3 satellite series is China's first civilian high-resolution stereo mapping satellite system [16]. To date, the launched ZY-3 satellites (01, 02, and 03) operate in sun-synchronous orbits and are equipped with three panchromatic cameras (forward-, backward-, and nadir-looking), enabling tri-linear array push-broom imaging and the generation of high-precision stereo mapping products [17,18]. Among them, the spatial resolution of the forward- and backward-looking cameras of ZY3-02/03 has been improved to 2.5 m, significantly enhancing their capability to resolve terrain details [19]. To obtain recent glacier topography in the study area, nine pairs of ZY3-02/03 tri-stereo images acquired between October 2024 and March 2025 were used in this study. During data selection, a cloud cover threshold of 5% was applied to minimize DEM voids caused by cloud contamination. The spatial coverage of these images is shown by the dark red rectangles in Figure 1, and their detailed parameters are listed in Table 1.

Table 1. Parameters of ZY-3 tri-stereo optical imagery used in this study.

Acquisition Date	Sensor	Cloud Cover (%)	Path/Row	Study Area
19 March 2024	ZY3-2	0	62/135	A
29 January 2025	ZY3-3	0	61/135	A
29 January 2025	ZY3-3	0	61/141	B
3 February 2025	ZY3-3	0	60/141	B
8 October 2024	ZY3-3	0	58/142	C
16 December 2024	ZY3-3	0	58/142	C
28 March 2025	ZY3-2	0	57/142	C
6 November 2024	ZY3-2	5	51/141	D
12 January 2024	ZY3-2	0	40/138	E

In this study, the Shuttle Radar Topography Mission (SRTM) DEM acquired in February 2000 was selected as the reference topographic dataset. The SRTM was equipped with both C-band (5.6 cm) and X-band (3.1 cm) radar systems [20]. In theory, the penetration capability of the X-band signal in glacierized areas is much weaker than that of the C-

band, making the X-band DEM more suitable for glacier change monitoring. However, the SRTM-X DEM has a swath width of only 50 km, resulting in substantial data gaps and insufficient coverage in the study area. To ensure complete spatial coverage, the C-band SRTM DEM with a spatial resolution of 30 m was ultimately selected. The data were obtained from the United States Geological Survey (USGS, USA). In addition, previous studies have shown that the penetration effect of the C-band radar signal in snow and ice is an important source of a systematic error [21], which will be specifically corrected during subsequent processing.

The Randolph Glacier Inventory version 7.0 (RGI 7.0) was used as the baseline dataset for glacier distribution in this study [22]. The RGI database is compiled based on the results of the World Glacier Monitoring Service and is internationally authoritative, with its latest release provided by the Global Land Ice Measurements from Space (GLIMS) initiative (National Snow and Ice Data Center, Boulder, CO, USA). To better match the baseline epoch of early 2000, glacier termini of non-surging glaciers in five study regions were manually corrected using cloud-free Landsat imagery from 1999/2000. For surging glaciers, the termini were updated using Landsat imagery temporally consistent with the ZY3 acquisitions, thereby obtaining glacier boundaries that were consistent with the study period.

To further analyze the impact of climate change on glacier mass balance, this study employed the ERA5-Land reanalysis dataset, obtained from the Copernicus Climate Change Service (https://cds.climate.copernicus.eu/datasets (accessed on 10 March 2026)) [23]. ERA5-Land provides hourly near-surface meteorological variables at a spatial resolution of $0.1^\circ \times 0.1^\circ$ (approximately 10 km) and covers the period from 1950 to near real time. It is generated by replaying the ECMWF's ERA5 atmospheric forcing through the Tiled ECMWF Scheme for Surface Exchanges over Land (HTESSEL) land surface model, and has been widely validated for hydrological and cryospheric studies in High Mountain Asia. In this study, the monthly aggregated ablation-season (May–September) mean temperature and annual precipitation data over the Three-River Headwaters Region from 2000 to 2025 were extracted and statistically analyzed. Linear trend analysis was applied to investigate regional climatic trends and their relationship with glacier mass balance changes, thereby providing a climatic context for the observed glacier surface elevation changes.

3.2. Methods

Figure 2 presents the complete technical workflow from multi-source data input to final mass balance estimation and hydrological contribution analysis. This workflow summarizes the core data processing procedures, error control steps, and key analytical components of this study, mainly including: (1) multi-temporal DEM generation and preprocessing based on SRTM and ZY-3 imagery; (2) derivation of reliable glacier surface elevation changes through co-registration, differencing, and systematic error correction; (3) estimation of glacier mass balance based on elevation changes and glacier inventory data, along with uncertainty analysis; and (4) integration of climate and runoff data to reveal the spatiotemporal characteristics of mass balance and evaluate its hydrological contribution. The following sections provide a detailed description of each step in accordance with this workflow.

3.2.1. DEM Generation, Co-Registration, and Differencing

In this study, the recent high-resolution digital elevation models (DEMs) were generated from ZY-3 tri-stereo optical imagery and differenced with the SRTM-C DEM acquired in early 2000 to obtain glacier surface elevation changes. The ZY3-02 and ZY3-03 tri-stereo optical images used for DEM generation were acquired between October 2024 and March

2025, with detailed parameters listed in Table 1. All images were selected with a cloud cover threshold of 5% or less to minimize DEM voids caused by cloud contamination. The ZY3 DEMs were generated using the Space Data Processor (SDP v1.0) software developed by the Land Satellite Remote Sensing Application Center of the Ministry of Natural Resources of China. Dense stereo matching and tri-image reconstruction methods were employed to ensure reliable feature matching even in steep and texture-poor glacierized areas [24].

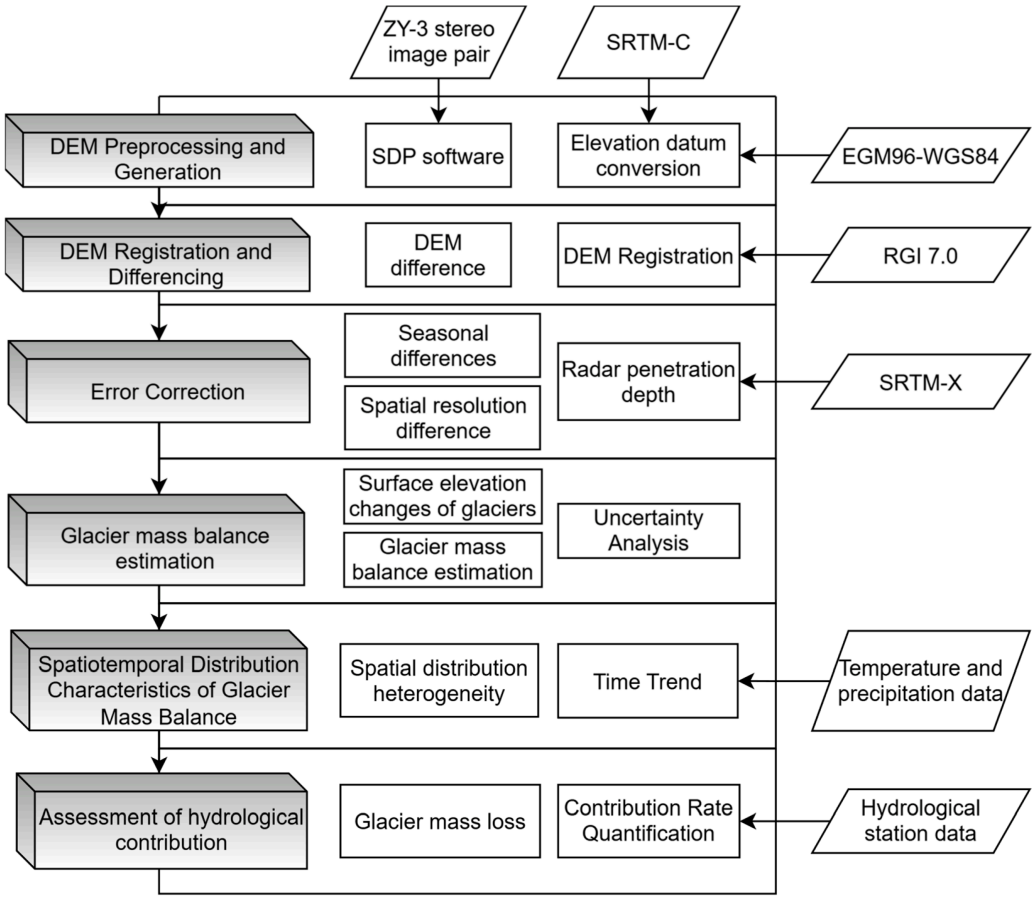

Figure 2. Technical workflow for estimating glacier mass balance from multisource remote sensing data.

To accurately compute elevation differences between DEMs from two periods, it is essential to first eliminate vertical biases induced by horizontal offsets between them [25]. Before DEM co-registration and differencing, the vertical datum of the SRTM DEM was converted from the EGM96 geoid to the WGS84 ellipsoid to ensure consistency with the ZY-3 DEM. This conversion was performed by adding the EGM96 geoid undulation to the SRTM orthometric height at each pixel. The geoid undulation values were interpolated from the EGM96 geoid model grid. In this study, the universal co-registration method proposed by Nuth and Kääb was applied to precisely align all ZY3 DEMs with the SRTM-C DEM [26]. The co-registered ZY3 DEMs were then subtracted from the SRTM-C DEM to obtain preliminary elevation change grids. These grids were masked using glacier boundaries from the Randolph Glacier Inventory version 7.0 (RGI 7.0) to extract elevation changes over glacierized areas.

Following the method of Liu et al., glacier pixels with slopes greater than 25° were excluded before calculating the mean elevation changes [27]. In addition, to identify and remove outliers, thresholds of ±150 m and ±200 m were applied to elevation change results

for non-surging and surging glaciers, respectively. Consistent with the DEM generation strategy, voids in the final elevation change maps were not filled by interpolation.

3.2.2. Systematic Error Corrections

To accurately extract true glacier surface elevation changes from DEM differencing results, systematic biases between multi-source DEM datasets must be corrected. In this study, three types of systematic errors were addressed, including those induced by radar penetration depth, spatial resolution differences, and seasonal acquisition discrepancies.

The C-band radar signal of SRTM exhibits a certain degree of penetration into snow and ice, resulting in measured surface elevations that are lower than the actual glacier surface. To correct this bias, the SRTM X-band DEM, acquired simultaneously but with much weaker penetration capability, was used for estimation. In theory, the elevation difference between the C-band and X-band DEMs can be approximated as the penetration depth of the C-band signal into glacier surfaces [28–30]. During correction, a functional relationship between penetration depth and elevation was first established based on elevation differences between the SRTM-C and SRTM-X DEMs, and this model was subsequently applied to each glacier pixel. For the Serfeng region, where SRTM-X data coverage is lacking, the penetration correction values were derived from fitted models of the adjacent Geladandong and Dongkemadi regions.

Even after precise co-registration, DEMs with different spatial resolutions may still exhibit systematic elevation biases in complex terrain. In this study, the method proposed by Gardelle et al. was adopted, which demonstrated that such biases are strongly correlated with maximum curvature (MC) of the terrain and exhibit consistent behavior in both glacierized and non-glacierized areas [21]. Therefore, a regression model between elevation residuals and maximum curvature in non-glacierized areas can be established and used to correct elevation biases in glacierized areas. The correction formula is as follows:

$$dh_2 = dh_1 - f(MC), \tag{1}$$

where dh_1 represents the elevation difference before correction, dh_2 represents the corrected elevation difference, and $f(MC)$ denotes the relationship between elevation residuals in non-glacierized areas and the maximum curvature of the terrain.

The SRTM-C DEM used as the reference dataset in this study was acquired in February 2000, whereas the ZY3-derived DEMs were mainly obtained during the winter months of 2024–2025 (October to March). For summer-accumulation-type glaciers in the study region, both the accumulation and ablation processes primarily occur during the ablation season, and glacier mass changes in winter are minimal. Therefore, although there is a temporal difference of several months between the two DEM datasets, the systematic bias introduced by seasonal mass changes is negligible in this study and was not corrected.

3.2.3. Estimation of the Average Glacier Surface Elevation Change

After obtaining the glacier elevation change results from DEM differencing between different periods, to further estimate the regional average change, we accurately calculated the mean value within 100 m elevation bins, based on the assumption that glacier pixels within a given elevation range generally experience similar elevation changes [31]. Accordingly, the average glacier elevation change (ΔH) was calculated using Equation (2). To minimize the impact of random errors, we averaged the elevation changes for each elevation interval using pixels with elevation change values within three times the standard deviation of the mean.

$$\Delta H = \frac{\sum dh_i \times S_i}{S_{\text{total}}} = \frac{\sum dh_i \times N_i}{\sum N_i}, \tag{2}$$

where ΔH denotes the overall average elevation change value of the glacierized area; S_i and S_{total} represent the glacier area within the i-th elevation bin and the total glacier area, respectively; dh_i is the average elevation change in the corresponding bin; and N_i is the number of pixels within this elevation bin.

3.2.4. Glacier Mass Balance Estimation and Uncertainty Analysis

Due to the harsh climatic conditions in High Mountain Asia, field observation opportunities are extremely limited and field surveys are very difficult, resulting in a lack of in situ measurements of glacier ice density within the time range of DEM acquisition. At present, among the methods for estimating glacier mass balance based on multi-source remote sensing data, the geodetic method is the most widely used. The basic principle of this method is to calculate elevation changes by comparing DEM data acquired in different periods for the same area, and then estimate the glacier mass balance in combination with the glacier area and average ice density. The estimation formula is as follows:

$$\Delta B = \frac{(\Delta H - P_C - f(MC)) \times \rho_{\text{glac}}}{T \times \rho_w}, \tag{3}$$

where ΔH, P_C, and $f(MC)$ represent the average glacier elevation change, the penetration depth of C-band radar signal, and the correlation between elevation residuals in non-glacierized areas and the maximum surface curvature, respectively; T is the number of integer years of the study period; ρ_{glac} (850 kg m^{-3}) is the conversion coefficient; and ρ_w (1000 kg m^{-3}) is the density of water.

We assessed the uncertainty of glacier mass balance for the entire TRHR using the glacier mass balance errors of the five study sites. Based on the standard law of error propagation, the uncertainty of glacier mass balance ($\sigma_{\Delta B}$) at the study sites mainly comes from the errors in average glacier elevation change, X-band radar penetration depth, and the conversion coefficient.

$$\sigma_{\Delta B} = \frac{\sqrt{(\Delta H - P_C - f(MC))^2 \times \sigma^2_{\rho_{\text{glac}}} + \left(\sigma^2_{\Delta H} + \sigma^2_{P_C}\right) \times \rho^2_{\text{glac}}}}{T \times \rho_w}, \tag{4}$$

where $\sigma_{\rho_{\text{glac}}}$ is the error of the conversion coefficient. Huss suggested that $\sigma_{\rho_{\text{glac}}}$ (± 60 kg·m^{-3}) is approximately 7% of the conversion coefficient [32]. σ_{P_C} is the error of the C-band radar penetration depth. Here, we analyzed the difference in penetration depth within each 100 m elevation bin, established a linear model between elevation and radar penetration, and characterized σ_{P_C} using the normalized median absolute deviation (NMAD). In addition, when calculating the average elevation change for each elevation interval, we selected elevation change values with a deviation from the mean value of less than three times the standard deviation to minimize the influence of random errors. Furthermore, $\sigma_{\Delta H}$ is the error of the average glacier elevation change at the study site.

$$\sigma_{\Delta H} = \sqrt{\frac{\sum\left(\sigma^2_{\Delta H_i} \cdot S_i^2\right)}{S^2_{\text{total}}} + \frac{(\Delta H^2) \cdot \sigma^2_{S_{\text{total}}}}{S^2_{\text{total}}}}, \tag{5}$$

where S_{total} is the uncertainty of the total glacier area (assumed to be $\pm 5\%$) [33], and $\sigma_{\Delta H_i}$ is the statistical uncertainty of the elevation change in the i-th elevation band. For each elevation interval, $\sigma_{\Delta H_i}$ can be calculated as follows:

$$\sigma_{\Delta H_i} = \frac{STDV_i}{\sqrt{N_{eff_i}}}, \tag{6}$$

where $STDV_i$ is the standard deviation of elevation changes within the i-th elevation band and N_{eff_i} is the number of independent pixels within that band, reflecting the effect of spatial autocorrelation.

Since adjacent pixels in remote sensing DEM data often exhibit spatial autocorrelation, directly using the total number of pixels as the degrees of freedom would underestimate uncertainty. Therefore, following Bolch et al. [34], the number of independent pixels is defined as follows:

$$N_{eff_i} = \frac{N_i \times PS}{2D}, \quad (7)$$

where N_i is the total number of pixels within the elevation band, PS is the DEM pixel resolution, and D is the spatial autocorrelation distance. Empirical studies indicate that D is approximately 20 times the pixel resolution; therefore, the number of independent pixels in each elevation band can be approximated as 1/40 of the total pixel count.

3.2.5. Analysis of Long-Term Trends in Climate Data

Considering that the glaciers investigated in this study are summer-accumulation type glaciers, whose mass accumulation and ablation processes mainly occur during the ablation season (May–September), we focused on estimating the interannual trends of annual precipitation and ablation season mean temperature from 2000 to 2025. The temporal trends of climate variables were estimated using linear regression analysis. Specifically, for each study area, climate time series data (such as ablation season mean temperature and annual precipitation) were fitted using linear regression to obtain the first-order coefficient of the regression equation (i.e., the annual rate of change). The decadal trend was calculated as ten times this coefficient, representing the average change in the climate variable per decade. This analytical approach aims to reveal the evolution characteristics of the climatic background in TRHR over the past 25 years, thereby providing a climate-driven explanation for the spatial heterogeneity and temporal variation in glacier mass balance during the same period.

4. Results

4.1. Glacier Surface Elevation Change

Based on the differencing results between the 2000 SRTM-C DEM and the 2024–2025 ZY-3 DEM, this study obtained the spatial distribution of glacier surface elevation changes in five key study areas of the TRHR during 2000–2025 (Figure 3). Glacier surfaces in the study area are dominated by thinning and exhibit a clear elevation dependency. The thinning rates in low-elevation areas (mainly glacier tongues) are generally higher than those in high-elevation areas (accumulation zones). Notably, slight surface lowering or even ice thickening was observed in several of the highest elevation bands (usually near ridge lines) across different study areas.

In Figure 3, panels A through E correspond to the Kunlun, Geladandong, Dongkemadi, Serfeng, and Animaqing regions, respectively (see Figure 1 for locations). In Kunlun, glaciers in the northwest exhibit intense ablation, whereas those in the southwest show an accumulation trend, suggesting that a surge event occurred in this area. In Geladandong, the glacier tongues generally present a strong ablation trend, and a glacier on the western side also exhibits surging characteristics. Dongkemadi has a relatively slow overall ablation rate, with no surge glaciers identified. In Serfeng, the tongues of fragmented glaciers are mostly oriented northward, but this area experiences the strongest ablation, and no surge glaciers are found. In Animaqing, glaciers in the northeastern part exhibit severe ablation, while those in the southwestern part show relatively slow ablation; a surge event is also identified on a glacier on the southwestern side.

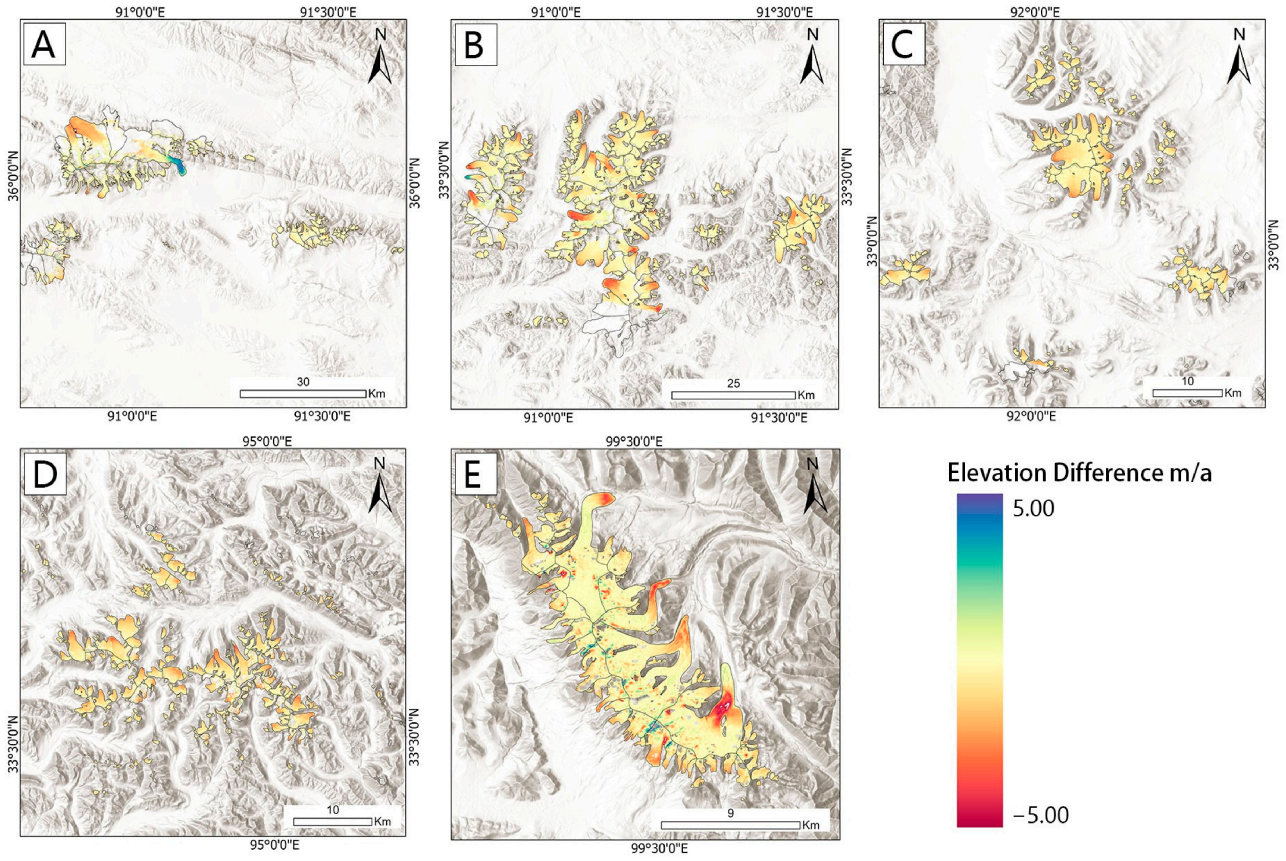

Figure 3. Spatial distribution of glacier surface elevation change rates in TRHR from 2000 to 2025. ((**A**–**E**) represent the five study regions: Kunlun, Geladandong, Dongkemadi, Serfeng, and Animaqing, respectively; the color scale indicates annual elevation change rates; blue tones represent thickening, red tones thinning. Glacier boundaries are derived from RGI 7.0 with manual corrections).

As described above, three surge-type glaciers were identified in the study area: one on the southeastern side of the Kunlun region, one on the western flank of the Ge-ladandong region, and one on the southwestern side of the Animaqing region. Instead of thinning at lower elevations and stability or slight thickening at higher elevations, all three surge glaciers show upper-part thinning and lower-tongue thickening during the study period. Specifically, in the Kunlun region, the southeastern glacier displays clear thickening in its lower tongue despite an otherwise moderate mass loss rate in the surrounding area. In the Geladan-dong region, the western glacier exhibits pronounced thinning in its upper part and thickening in the lower tongue. In the Ani-maqing region, a similar but less pronounced pattern is observed on the southwestern side. These abnormal changes, though locally confined, provide critical evidence for understanding surge dynamics in the TRHR.

4.2. Glacier Mass Loss

During 2000–2025, glacier mass balance in TRHR exhibited an overall negative trend, with significant differences among regions (Table 2). Within the Yangtze River source region, the degree of glacier mass loss varies among different study areas. Among them, the northern part of the Serfeng region shows the highest mass loss rate, reaching -0.73 ± 0.07 m w.e. yr^{-1}; the southern part of the Serfeng region exhibits a mass loss rate of -0.70 ± 0.07 m w.e. yr^{-1}; Dongkemadi follows with -0.56 ± 0.06 m w.e. yr^{-1}; while Kunlun and Geladandong show relatively lower mass loss rates of -0.40 ± 0.06 m w.e. yr^{-1} and -0.41 ± 0.06 m w.e. yr^{-1}, respectively. The overall mass loss rate for the entire Serfeng region is -0.72 ± 0.07 m w.e. yr^{-1} (Table 2).

Table 2. Glacier mass balance in different subregions of TRHR from 2000 to 2025.

Region	Mass Balance (m w.e. yr^{-1})
Kunlun	-0.40 ± 0.06
Geladandong	-0.41 ± 0.06
Dongkemadi	-0.56 ± 0.06
Serfeng [1]	-0.73 ± 0.07
Serfeng [2]	-0.70 ± 0.07
Animaqing	-0.37 ± 0.09
TRHR *	-0.46 ± 0.06

Serfeng [1] represents the northern part of the Serfeng region (Northern Serfeng), and Serfeng [2] represents the southern part of the Serfeng region (Southern Serfeng). * The value for TRHR is calculated as the area-weighted mean of the subregions.

As shown in Table 2, the five study areas display a clear gradient of glacier mass loss. The Serfeng region exhibits the most negative mass balance (-0.72 ± 0.07 m w.e. yr^{-1}), followed by Dongkemadi (-0.56 ± 0.06 m w.e. yr^{-1}). Geladandong (-0.41 ± 0.06 m w.e. yr^{-1}) and Kunlun (-0.40 ± 0.06 m w.e. yr^{-1}) show moderate levels of mass loss, while the Animaqing region records the least negative balance (-0.37 ± 0.09 m w.e. yr^{-1}). The northern and southern parts of the Serfeng region show very similar mass loss rates (-0.73 vs. -0.70 m w.e. yr^{-1}), both within uncertainty, and are therefore treated as a single unit (Serfeng) in the following discussion. These results indicate that glaciers across the TRHR are generally in a state of mass deficit with pronounced spatial heterogeneity, with mass loss rates ranging from -0.72 to -0.37 m w.e. yr^{-1} among the five subregions. Notably, the Serfeng region (located in the Lancang River source) suffers the most severe ablation, whereas the Animaqing region (in the Yellow River source) experiences the weakest mass loss.

5. Discussion

5.1. Climatic Driving Mechanisms of the Spatial Differentiation of Glacier Mass Balance

From the perspective of climatic background, the spatial differentiation of glacier mass balance results from the combined effects of precipitation and temperature—precipitation influences mass accumulation, while ablation-season temperature dominates the ablation process. Between 2000 and 2025, annual precipitation in all study areas showed an increasing trend (Figure 4), and the ablation-season mean temperatures also generally increased (Figure 5). However, the combinations of decadal change rates varied significantly among regions, thereby shaping the regional pattern of glacier ablation. Overall, regions with higher warming rates and relatively limited precipitation increases experienced the most severe mass loss, whereas regions with lower warming rates or more pronounced precipitation increases exhibited relatively weaker ablation.

In the Serfeng region, annual precipitation increased at a rate of +19.96 mm·$10a^{-1}$ (approximately +4.6% per decade), while ablation-season mean temperature increased at +0.62 °C·$10a^{-1}$. Despite the increase in precipitation, the strong warming dominated the ablation process, driving the glacier mass loss rate in this region to the highest level, reaching -0.72 ± 0.07 m w.e. yr^{-1}. In the Dongkemadi region (southern Yangtze River source), the warming rate was also relatively high (+0.68 °C·$10a^{-1}$), with a precipitation increase of +9.59 mm·$10a^{-1}$ (approximately +2.5% per decade), resulting in a moderate-to-high mass loss of -0.56 ± 0.06 m w.e. yr^{-1}. The Kunlun region (northern Yangtze River source) showed a different climatic combination: precipitation increased at +17.25 mm·$10a^{-1}$ (approximately +6.0% per decade), but the ablation-season temperature rise was relatively lower (+0.68 °C·$10a^{-1}$). Coupled with its inherently low temperature baseline, the ablation forcing was weaker, leading to a smaller mass loss of -0.40 ± 0.06 m w.e. yr^{-1}. The

Animaqing region (Yellow River source) represents another typical case: it exhibited the highest precipitation increase rate (+24.26 mm·10a^{-1}, approximately +5.4% per decade) and the lowest warming rate among all regions (+0.44 °C·10a^{-1}). The relatively high precipitation baseline provided favorable conditions for mass accumulation, partially buffering the mass loss, making it the region with the weakest ablation (-0.37 ± 0.09 m w.e. yr^{-1}). The Geladandong region (southern Yangtze River source) showed intermediate levels for all trend indicators (precipitation: +7.81 mm·10a^{-1}, approximately +2.2% per decade; temperature: +0.73 °C·10a^{-1}), and its mass balance result was correspondingly moderate (-0.41 ± 0.06 m w.e. yr^{-1}).

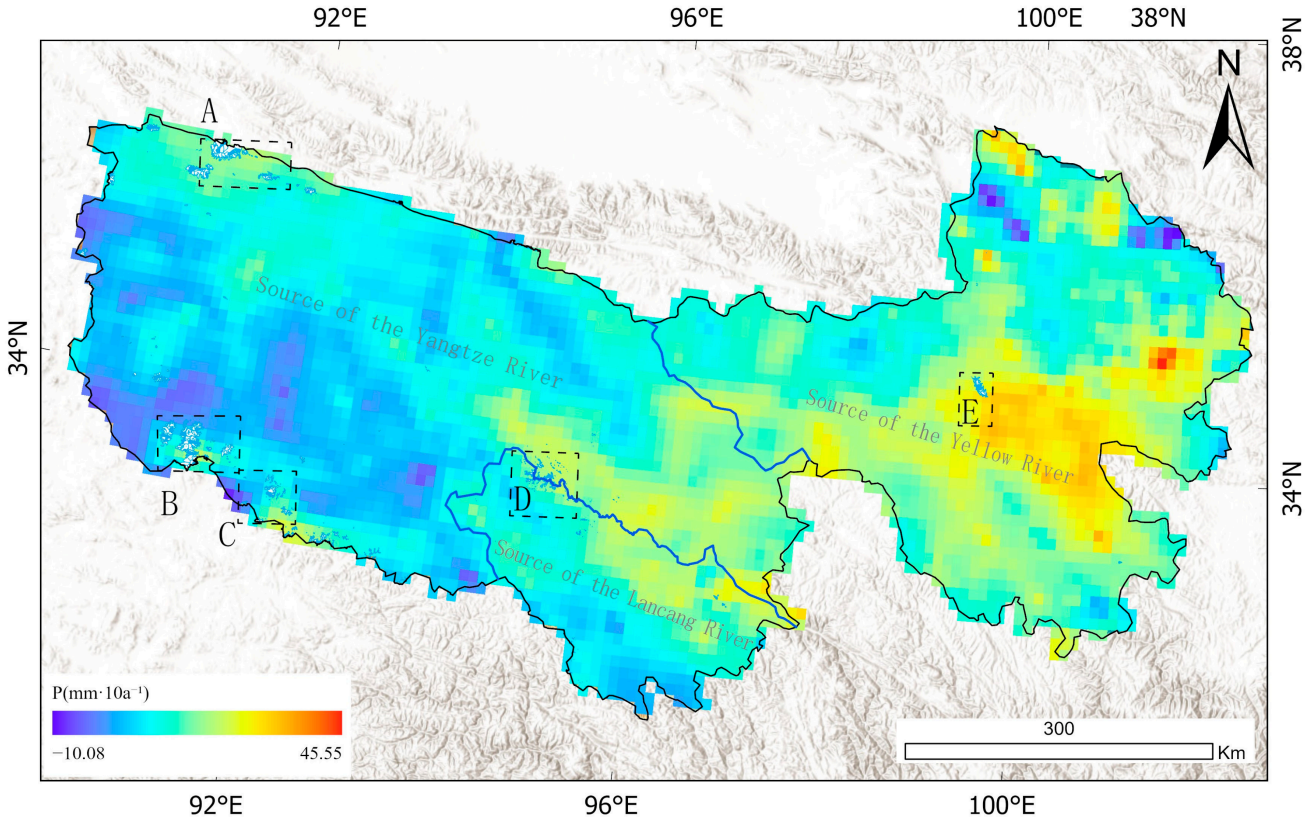

Figure 4. Decadal trends in annual mean precipitation (mm·10a^{-1}) in the five study areas of TRHR from 2000 to 2025. ((A–E) represent the five study regions: Kunlun, Geladandong, Dongkemadi, Serfeng, and Animaqing, respectively).

5.2. Acceleration of Glacier Mass Loss and Its Climatic Causes

Compared with previous estimates based on data from 2000 to 2018, the glacier mass balance results for 2000–2025 obtained in this study indicate a general acceleration of glacier mass loss across all sub-regions of the Three-River Headwaters Region (Table 3). Further analysis of the changes in climatic variables before and after 2018 (Tables 4 and 5) reveals that the magnitude of acceleration is closely related to the regional warming rate and the increase in precipitation; regions with stronger warming and limited precipitation increases experienced more pronounced acceleration of mass loss, whereas regions with weaker warming and larger precipitation increases showed relatively milder acceleration. In addition, differences in the spatial extent of study areas may also lead to apparent discrepancies in glacier change rates.

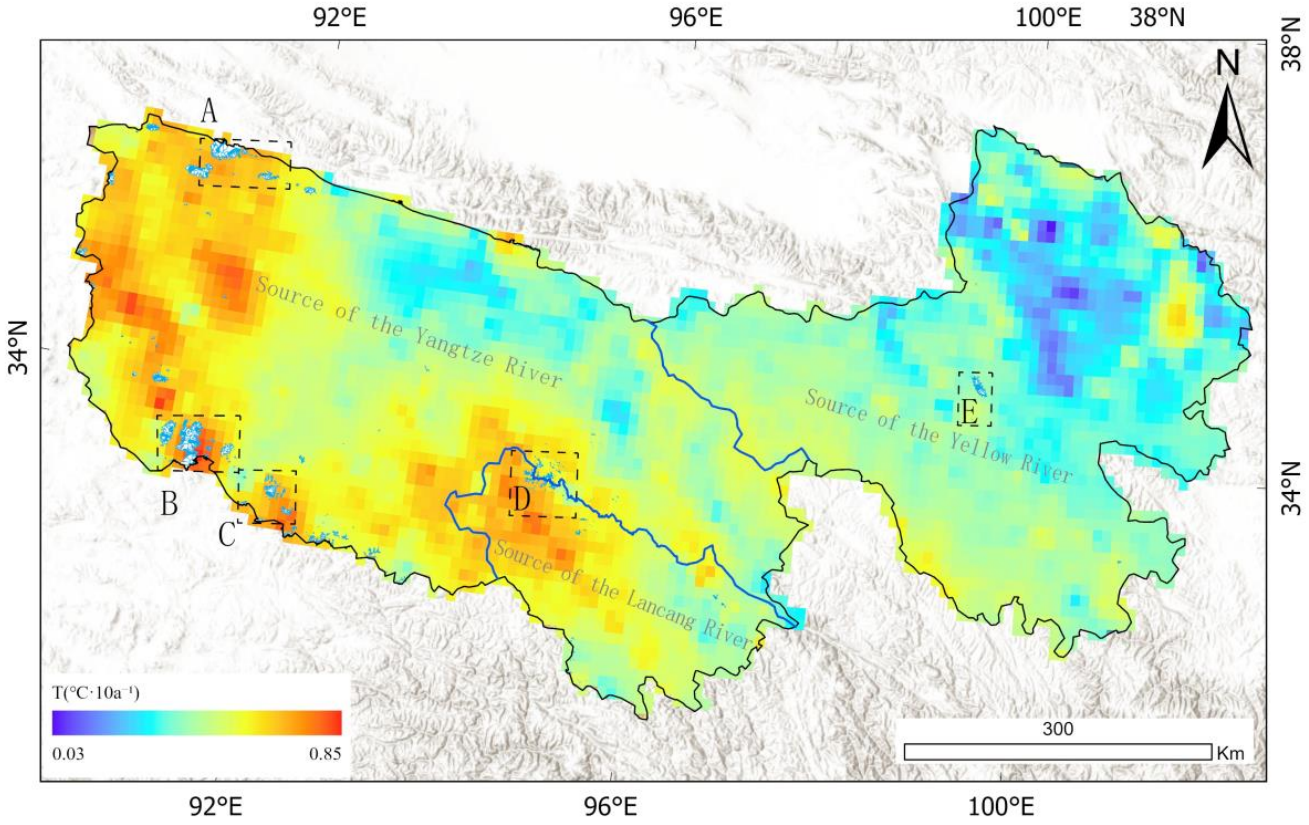

Figure 5. Decadal trends of ablation season mean temperature (°C·10a^{-1}) in the five study areas of TRHR from 2000 to 2025. ((A–E) represent the five study regions: Kunlun, Geladandong, Dongkemadi, Serfeng, and Animaqing, respectively).

Table 3. Comparison of glacier mass-balance estimates between this study and previous studies.

Region	This Study (2000–2025) (m w.e. yr^{-1})	Previous Studies (2000–2018) (m w.e. yr^{-1})	References
Kunlun	−0.40 ± 0.06	−0.07 ± 0.07	Shean et al., 2020 [35]
Geladandong	−0.41 ± 0.06	−0.20 ± 0.07	Liu et al., 2020 [7]
Dongkemadi	−0.56 ± 0.06	−0.45 ± 0.10	
Serfeng	−0.72 ± 0.07	−0.59 ± 0.13	
Animaqing	−0.37 ± 0.09	−0.36 ± 0.06	Zhou et al., 2022 [36]

Table 4. Comparison of annual mean precipitation (mm) before (2000–2018) and after (2019–2025) 2018 across the five study areas in the Three-River Headwaters Region.

Region	Average Precipitation Before 2018 (mm)	Average Precipitation After 2018 (mm)	Change (mm)
Kunlun	284.3	305.8	21.5
Geladandong	360.9	365.2	4.3
Dongkemadi	375.4	386.9	11.5
Serfeng	420.7	465.6	44.9
Animaqing	432.1	483.1	51.0

Table 5. Comparison of ablation-season mean temperature (°C) before (2000–2018) and after (2019–2025) 2018 across the five study areas in the Three-River Headwaters Region.

Region	Average Temperature Before 2018 (°C)	Average Temperature After 2018 (°C)	Change (°C)
Kunlun	−2.81	−1.85	0.96
Geladandong	−2.11	−0.99	1.12
Dongkemadi	−0.09	1.05	1.14
Serfeng	−0.42	0.57	0.99
Animaqing	1.21	1.91	0.70

Among the five study areas, Geladandong exhibits the most prominent acceleration of glacier mass loss, with the mass balance rate decreasing from −0.20 m w.e. yr^{-1} during 2000–2018 to −0.41 m w.e. yr^{-1} during 2000–2025. According to Table 5, the ablation-season mean temperature in this area increased by +1.12 °C after 2018 (from −2.11 °C to −0.99 °C), representing one of the largest warming magnitudes among the five regions. Meanwhile, the annual precipitation increased by only 4.3 mm (Table 4), which is far from sufficient to offset the enhanced ablation driven by warming. Consequently, Geladandong shows the strongest acceleration of glacier mass loss in the study region. The Serfeng region (Area D) ranks second in terms of acceleration, with the mass loss rate increasing from −0.59 m w.e. yr^{-1} to −0.72 m w.e. yr^{-1}. In this region, the ablation-season mean temperature rose by +0.99 °C (Table 5), and precipitation increased by 44.9 mm (Table 4). Although the precipitation increase is relatively large, the dominant role of warming still leads to a continued net mass loss, resulting in a pronounced acceleration. Dongkemadi (Area C) shows a mass loss acceleration from −0.45 m w.e. yr^{-1} to −0.56 m w.e. yr^{-1}. This area experienced the largest warming of ablation-season mean temperature among all five regions (+1.14 °C, Table 5), but only a modest precipitation increase of 11.5 mm (Table 4), which is insufficient to buffer the intensified ablation. Therefore, its acceleration is slightly lower than that of Serfeng but remains substantial. Animaqing (Area E) exhibits the weakest acceleration of glacier mass loss, with the mass balance rate decreasing only slightly from −0.36 m w.e. yr^{-1} to −0.37 m w.e. yr^{-1}. According to Table 5, this region has the smallest warming of ablation-season mean temperature (+0.70 °C), and Table 4 shows the largest precipitation increase (51.0 mm). The relatively mild warming combined with a significant increase in precipitation effectively enhances glacier accumulation and buffers the ablation caused by climate warming, making Animaqing the region with the least mass loss and the weakest acceleration.

It is worth noting that the mass loss rate in the Kunlun region (Area A) obtained in this study (-0.40 ± 0.06 m w.e. yr^{-1}) differs markedly from the estimate of Shean et al. (2020) [35] for the entire Kunlun Shan range on a macro scale (-0.07 ± 0.07 m w.e. yr^{-1}). This discrepancy is not primarily due to temporal acceleration after 2018, but rather to differences in spatial definition: Area A in this study represents a specific local sector on the southern slope of the eastern Kunlun Mountains, whereas Shean et al. defined the "Kunlun" region to encompass the entire mountain range. This comparison highlights the strong spatial heterogeneity of the glacier response to climate change in the Kunlun Mountains.

In summary, since 2018, the Three-River Headwaters Region has experienced an overall "warmer and wetter" trend, but the combination of warming and wetting varies significantly among sub-regions, directly leading to a differentiated pattern of glacier mass loss acceleration. Warming plays the dominant role, while increased precipitation exerts a buffering effect [37]. Geladandong, Serfeng, and Dongkemadi exhibit successively high levels of acceleration, whereas Animaqing shows the weakest acceleration due to its mild warming and abundant precipitation increase. These findings deepen our understanding

of the climatic driving mechanisms behind the spatiotemporal evolution of glaciers in the Three-River Headwaters Region.

5.3. Contribution of Glacier Mass Loss to Annual River Runoff

The contribution of glacier mass loss to river runoff is a key issue for understanding hydrological processes and water resource evolution in cold regions. Based on the estimated glacier mass balance results for the source regions of TRHR during 2000–2025 (Table 6) combined with basin hydrological observation data, this study quantitatively analyzes the contribution of glacier ablation to annual runoff in the source regions of the Yangtze River, Yellow River, and Lancang River.

Table 6. Glacier mass balance and glacier mass loss in the TRHR from 2000 to 2025.

Region	Effective Glacier Area (km^2)	Mass Balance (m w.e. yr^{-1})	Mass Loss (Gt yr^{-1})
Yangtze River source	1728.54	-0.45 ± 0.06	-0.778 ± 0.104
Lancang River source	106.67	-0.70 ± 0.07	-0.075 ± 0.007
Yellow River source	90.77	-0.37 ± 0.09	-0.039 ± 0.010

The sources and processing of runoff data for each basin are as follows: for the Yangtze River source region, the annual mean runoff of the Tongtian River at the Zhimenda hydrological station during 2000–2018, 17.84 Gt yr^{-1}, is adopted [35]; for the Yellow River source region, the long-term mean runoff of 20.7 Gt yr^{-1} recorded at the Tangnaihai station during 1960–2020 is used [38]; for the Lancang River source region, the annual mean runoff of 23.49 Gt yr^{-1} at the Zhongwunonglong section during 2000–2019 is selected [39]. Although the runoff observation series does not fully extend to 2025, considering that interannual runoff variability is mainly controlled by climatic cycles, and that this study focuses on long-term average contribution ratios, the above long-term mean runoff values can reasonably represent the overall runoff level during 2000–2025 under relatively stable climatic conditions. In addition, the contribution rate of glacier meltwater is not sensitive to the absolute magnitude of runoff, and its estimation mainly reflects the relative importance at the order-of-magnitude level.

The contribution rates of glacier mass loss to annual runoff vary significantly among the source regions of TRHR. The Yangtze River source region shows the highest contribution rate (4.4%), which is related to its large glacier area, strong ablation intensity, and moderate runoff magnitude. The contribution rates in the Yellow River and Lancang River source regions are both less than 0.5%, mainly due to two factors: first, the glacier areas in these two regions are much smaller than those in the Yangtze River source region, resulting in limited total glacier mass loss; second, their annual runoff is significantly higher than that of the Yangtze River source region (approximately 16–32% higher), and the large runoff baseline greatly dilutes the relative contribution of glacier meltwater. It is noteworthy that although the Lancang River source region exhibits the strongest glacier ablation rate (-0.70 m w.e. yr^{-1}), its contribution rate remains low because it has the largest runoff among the three source regions.

Overall, the area-weighted average contribution of glacier mass loss to annual runoff across the entire TRHR is less than 2% (e.g., 4.4% in the Yangtze River source versus <0.5% in the other two sources). This result clearly indicates that glacier meltwater is not the primary source of river runoff in TRHR, and that regional runoff is mainly dominated by precipitation changes. At the same time, this result is significantly lower than the previously estimated 11–17% based on empirical formulae, highlighting the reliability and necessity of glacier mass balance assessment using the high-precision geodetic method.

6. Conclusions

In this study, based on the geodetic method, we systematically estimated the glacier mass balance in TRHR from 2000 to 2025 using the 2000 SRTM-C DEM and 2024–2025 ZY-3 DEM. The results show that glaciers in this region are in an overall state of mass deficit with significant spatial heterogeneity: glaciers in the Lancang River source region experienced the strongest ablation (-0.70 ± 0.07 m w.e. yr^{-1}), those in the Yellow River source region had the mildest ablation (-0.37 ± 0.09 m w.e. yr^{-1}), and glaciers in the Yangtze River source region presented an intermediate level of mass loss (-0.45 ± 0.06 m w.e. yr^{-1}). The spatial differentiation of glacier mass loss is jointly regulated by changes in air temperature and precipitation, and generally shows a distribution pattern of stronger ablation in the south than in the north and more severe mass loss in the west than in the east.

Compared with the research results before 2018, glacier mass loss in most regions has intensified significantly from 2018 to 2025, with the most prominent changes being in the Geladandong, Dongkemadi and Serfeng regions. This indicates that, with the background of simultaneous increases in both regional air temperature and precipitation, rising temperature has played a dominant role in driving the accelerating glacier ablation, outweighing the mitigating effect of increased precipitation. The results of this study deepen the understanding of the spatiotemporal characteristics of glacier changes and their climate response mechanisms in TRHR, and can provide an important scientific basis for water resources management and ecological conservation in this region.

Author Contributions: Conceptualization, L.L.; methodology, D.L. and L.L.; validation, D.L. and L.L.; formal analysis, D.L. and L.L.; writing—original draft preparation, D.L., Y.L. and Z.L. (Zhengwei Li); writing—review and editing, D.L., X.Z., Z.L. (Zhicai Luo) and H.J.; funding acquisition, L.L. All authors have read and agreed to the published version of the manuscript.

Funding: This study was jointly supported by the CRSRI Open Research Program (CKWV2025958/KY) and the National Natural Science Foundation of China (42274028, 42274112).

Data Availability Statement: The SRTM-C DEM data are publicly available from the United States Geological Survey (USGS) at https://earthexplorer.usgs.gov/ (accessed on 17 September 2025). The ZY-3 tri-stereo optical imagery can be obtained from the Land Satellite Remote Sensing Application Center of the Ministry of Natural Resources of China. Glacier delineations are available from the Randolph Glacier Inventory version 7.0 (RGI 7.0) at https://www.glims.org/RGI/ (accessed on 17 September 2025). The Second Chinese Glacier Inventory data are available from the National Tibetan Plateau Data Center at https://www.tpdc.ac.cn. The ERA5-Land reanalysis dataset used for climate analysis can be accessed from the Copernicus Climate Change Service (C3S) at https://cds.climate.copernicus.eu/datasets (accessed on 10 March 2026).

Acknowledgments: The authors gratefully acknowledge the National Tibetan Plateau Data Center for providing the meteorological and glacier inventory datasets, and the USGS for providing the SRTM DEM. The authors also thank the anonymous reviewers and editors for their constructive comments, which substantially improved the quality of this manuscript.

Conflicts of Interest: The authors declare no conflicts of interest.

References

1. Sun, Q.L.; Li, B.L.; Li, F.; Zhang, Z.; Ding, L.; Zhang, T.; Xu, L. Review on the estimation of net primary productivity of vegetation in the Three-River Headwater Region, China. *Acta Geogr. Sin.* **2016**, *71*, 1596–1612.
2. Li, S.; Yao, Z.; Wang, R.; Liu, Z. Dryness/wetness pattern over the Three-River Headwater Region: Variation characteristic, causes, and drought risks. *Int. J. Climatol.* **2020**, *40*, 3550–3566.
3. Wang, S.; Fan, J.; Li, Y.; Wu, D.; Zhang, Y.; Huang, L. Dynamic response of water retention to grazing activity on grassland over the Three River Headwaters region. *Agric. Ecosyst. Environ.* **2019**, *286*, 106662. [CrossRef]

4. Ye, Q.; Wang, Y.; Liu, L.; Guo, L.; Zhang, X.; Dai, L.; Zhai, L.; Hu, Y.; Ali, N.; Ji, X.; et al. Remote sensing and modeling of the cryosphere in high mountain Asia: A multidisciplinary review. *Remote Sens.* **2024**, *16*, 1709. [CrossRef]
5. Liu, L.; Jiang, L.; Jiang, H.; Wang, H.; Ma, N.; Xu, H. Accelerated glacier mass loss (2011–2016) over the Puruogangri ice field in the inner Tibetan Plateau revealed by bistatic InSAR measurements. *Remote Sens. Environ.* **2019**, *231*, 111241. [CrossRef]
6. Liao, Y.; Liu, L.; Zhang, X. Evaluating the Performance of Multiple Machine Learning and Deep Learning Models on Glacier Mass Balance Estimation. *Symmetry* **2026**, *18*, 873. [CrossRef]
7. Liu, L.; Jiang, L.; Wang, H.; Ding, X.; Xu, H. Estimation of glacier mass loss and its contribution to river runoff in the source region of the Yangtze River during 2000–2018. *J. Hydrol.* **2020**, *589*, 125207. [CrossRef]
8. Chen, L.; Che, Y.; Cao, Y.; Wang, S.; Ma, X. Glacier mass balance based on two digital elevation models and ground observation records for the Baishui River Glacier No. 1 in Yulong Snow Mountain, Southeastern Qinghai–Tibet Plateau. *Front. Earth Sci.* **2022**, *10*, 883673. [CrossRef]
9. Che, Y.; Zhang, M.; Li, Z.; Wei, Y.; Nan, Z.; Li, H.; Wang, S.; Su, B. Energy balance model of mass balance and its sensitivity to meteorological variability on Urumqi River Glacier No. 1 in the Chinese Tien Shan. *Sci. Rep.* **2019**, *9*, 13958. [PubMed]
10. Wang, R.; Ding, Y.; Shangguan, D.; Cuo, L.; Zhao, Q.; Qin, J.; Li, J.; Song, M. Projections of glacier peak water and its timing in the Sanjiangyuan on the Tibet Plateau. *J. Hydrol. Reg. Stud.* **2023**, *45*, 101313. [CrossRef]
11. Falaschi, D.; Bhattacharya, A.; Guillet, G.; Huang, L.; King, O.; Mukherjee, K.; Rastner, P.; Yao, T.; Bolch, T. Annual to seasonal glacier mass balance in High Mountain Asia derived from Pléiades stereo images: Examples from the Pamir and the Tibetan Plateau. *Cryosphere* **2023**, *17*, 5435–5458. [CrossRef]
12. Wei, W.; Ke, Z.; Jie, Z. Review and prospect of human-land relationship in Three River Headwaters region: Based on the perspective of people, events, time and space. *Adv. Earth Sci.* **2020**, *35*, 26.
13. Liu, J.; Xu, X.; Shao, Q. Grassland degradation in the "three-river headwaters" region, Qinghai province. *J. Geogr. Sci.* **2008**, *18*, 259–273. [CrossRef]
14. Li, W.H.; Zhao, X.Q.; Zhang, X.Z.; Shi, P.L.; Wang, X.D.; Zhao, L. Change mechanism in main ecosystems and its effect of carbon source/sink function on the Qinghai-Tibetan Plateau. *Chin. J. Nat.* **2013**, *35*, 172–178.
15. Guo, W.; Liu, S.; Xu, J.; Wu, L.; Shangguan, D.; Yao, X.; Wei, J.; Bao, W.; Yu, P.; Liu, Q.; et al. The second Chinese glacier inventory: Data, methods and results. *J. Glaciol.* **2015**, *61*, 357–372. [CrossRef]
16. Pan, H.; Zhang, G.; Tang, X.; Li, D.; Zhu, X.; Zhou, P.; Jiang, Y. Basic Products of the ZiYuan-3 Satellite and Accuracy Evaluation. *Photogramm. Eng. Remote Sens.* **2013**, *79*, 1131–1145. [CrossRef]
17. Tang, X.; Zhang, G.; Zhu, X.; Pan, H.; Jiang, Y.; Zhou, P.; Wang, X. Triple linear-array image geometry model of ZiYuan-3 surveying satellite and its validation. *Int. J. Image Data Fusion* **2013**, *4*, 33–51.
18. Pan, H.; Tao, C.; Zou, Z. Precise georeferencing using the rigorous sensor model and rational function model for ZiYuan-3 strip scenes with minimum control. *ISPRS J. Photogramm. Remote Sens.* **2016**, *119*, 259–266. [CrossRef]
19. Xu, K.; Jiang, Y.; Zhang, G.; Zhang, Q.; Wang, X. Geometric potential assessment for ZY3-02 triple linear array imagery. *Remote Sens.* **2017**, *9*, 658. [CrossRef]
20. Rabus, B.; Eineder, M.; Roth, A.; Bamler, R. The shuttle radar topography mission—A new class of digital elevation models acquired by spaceborne radar. *ISPRS J. Photogramm. Remote Sens.* **2003**, *57*, 241–262. [CrossRef]
21. Gardelle, J.; Berthier, E.; Arnaud, Y. Impact of resolution and radar penetration on glacier elevation changes computed from DEM differencing. *J. Glaciol.* **2012**, *58*, 419–422. [CrossRef]
22. Maussion, F.; Butenko, A.; Champollion, N.; Dusch, M.; Eis, J.; Fourteau, K.; Gregor, P.; Jarosch, A.H.; Landmann, J.; Oesterle, F.; et al. The open global glacier model (OGGM) v1. 1. *Geosci. Model Dev.* **2019**, *12*, 909–931. [CrossRef]
23. Muñoz Sabater, J. ERA5-Land Monthly Averaged Data from 1950 to Present. Copernicus Climate Change Service (C3S) Climate Data Store (CDS). 2019. Available online: https://cds.climate.copernicus.eu/datasets/reanalysis-era5-land-monthly-means?tab=overview (accessed on 10 March 2026).
24. Xinming, T.; Qingxing, Y.; Xiaoming, G. China DSM Generation and Accuracy Acessment Using ZY3 Images. In *IGARSS 2018-2018 IEEE International Geoscience and Remote Sensing Symposium*; IEEE: New York, NY, USA, 2018; pp. 6757–6760.
25. Berthier, E.; Arnaud, Y.; Kumar, R.; Ahmad, S.; Wagnon, P.; Chevallier, P. Remote sensing estimates of glacier mass balances in the Himachal Pradesh (Western Himalaya, India). *Remote Sens. Environ.* **2007**, *108*, 327–338. [CrossRef]
26. Nuth, C.; Kääb, A. Co-registration and bias corrections of satellite elevation data sets for quantifying glacier thickness change. *Cryosphere* **2011**, *5*, 271–290. [CrossRef]
27. Liu, L.; Jiang, L.; Sun, Y.; Yi, C.; Wang, H.; Hsu, H. Glacier elevation changes (2012–2016) of the Puruogangri Ice Field on the Tibetan Plateau derived from bi-temporal TanDEM-X InSAR data. *Int. J. Remote Sens.* **2016**, *37*, 5687–5707.
28. Gardelle, J.; Berthier, E.; Arnaud, Y.; Kääb, A. Region-wide glacier mass balances over the Pamir-Karakoram-Himalaya during 1999–2011. *Cryosphere* **2013**, *7*, 1263–1286.
29. Zhou, Y.; Li, Z.; Li, J.I.A. Slight glacier mass loss in the Karakoram region during the 1970s to 2000 revealed by KH-9 images and SRTM DEM. *J. Glaciol.* **2017**, *63*, 331–342. [CrossRef]

30. Cao, B.O.; Pan, B.; Guan, W.; Wen, Z.; Wang, J.I. Changes in glacier volume on Mt. Gongga, southeastern Tibetan Plateau, based on the analysis of multi-temporal DEMs from 1966 to 2015. *J. Glaciol.* **2019**, *65*, 366–375. [CrossRef]
31. Berthier, E.; Arnaud, Y.; Baratoux, D.; Vincent, C.; Rémy, F. Recent rapid thinning of the "Mer de Glace" glacier derived from satellite optical images. *Geophys. Res. Lett.* **2004**, *31*, L17401. [CrossRef]
32. Huss, M. Density assumptions for converting geodetic glacier volume change to mass change. *Cryosphere* **2013**, *7*, 877–887. [CrossRef]
33. Paul, F.; Barrand, N.E.; Baumann, S.; Berthier, E.; Bolch, T.; Casey, K.; Frey, H.; Joshi, S.P.; Konovalov, V.; Le Bris, R.; et al. On the accuracy of glacier outlines derived from remote-sensing data. *Ann. Glaciol.* **2013**, *54*, 171–182. [CrossRef]
34. Bolch, T.; Pieczonka, T.; Benn, D.I. Multi-decadal mass loss of glaciers in the Everest area (Nepal Himalaya) derived from stereo imagery. *Cryosphere* **2011**, *5*, 349–358. [CrossRef]
35. Shean, D.E.; Bhushan, S.; Montesano, P.; Rounce, D.R.; Arendt, A.; Osmanoglu, B. A systematic, regional assessment of high mountain Asia glacier mass balance. *Front. Earth Sci.* **2020**, *7*, 363. [CrossRef]
36. Zhou, M.; Xu, S.; Wang, Y.; Wang, Y.; Hou, S. Recent 50-Year Glacier Mass Balance Changes over the Yellow River Source Region, Determined by Remote Sensing. *Remote Sens.* **2022**, *14*, 6286. [CrossRef]
37. Che, Y.; Wang, S.; Cao, Y.; Lv, W.; Ma, X.; Han, C.; Zhong, J.; Wu, R. Temperature sensitivity and rainfall heat flux drive rapid mass loss of low-latitude glaciers in the Southeastern Qinghai–Tibet Plateau. *Catena* **2026**, *267*, 109991.
38. Cui, C.; Chao, X. Analysis of Runoff Variation Laws at Multiple Time Scales in the Ma-Tang Section of the Yellow River Source Region. *Inn. Mong. Water Resour.* **2025**, *45*, 56–59. (In Chinese)
39. Li, H.; Zhang, P.; Guan, Z. Analysis of Runoff Evolution Characteristics in the Upper Reaches of the Lancang River in the Past 30 Years. *J. Yangtze River Sci. Res. Inst.* **2023**, *40*, 24–29. [CrossRef]